

Study of the Process $e^+e^- \rightarrow \pi^0\pi^0\gamma$ in c.m. Energy Range 600–970 MeV at CMD-2

R.R. Akhmetshin ^a, V.M. Aulchenko ^{a,b}, V.Sh. Banzarov ^a,
 A. Baratt ^c, L.M. Barkov ^{a,b}, S.E. Baru ^a, N.S. Bashtovoy ^a,
 A.E. Bondar ^{a,b}, D.V. Bondarev ^a, A.V. Bragin ^a,
 S.I. Eidelman ^{a,b}, D.A. Epifanov ^a, G.V. Fedotovitch ^{a,b},
 N.I. Gabyshev ^a, D.A. Gorbachev ^a, A.A. Grebeniuk ^a,
 D.N. Grigoriev ^a, F.V. Ignatov ^a, S.V. Karpov ^a, V.F. Kazanin ^a,
 B.I. Khazin ^{a,b}, I.A. Koop ^{a,b}, P.P. Krokovny ^a, A.S. Kuzmin ^{a,b},
 I.B. Logashenko ^a, P.A. Lukin ^a, A.P. Lysenko ^a,
 K.Yu. Mikhailov ^a, A.I. Milstein ^{a,b}, I.N. Nesterenko ^a,
 V.S. Okhupkin ^a, A.V. Otboev ^a, E.A. Perevedentsev ^{a,b},
 A.A. Polunin ^a, A.S. Popov ^a, S.I. Redin ^a, N.I. Root ^a,
 A.A. Ruban ^a, N.M. Ryskulov ^a, A.G. Shamov ^a,
 Yu.M. Shatunov ^a, B.A. Shwartz ^{a,b}, A.L. Sibidanov ^{a,b},
 V.A. Sidorov ^a, A.N. Skrinsky ^a, I.G. Snopkov ^a, E.P. Solodov ^{a,b},
 P.Yu. Stepanov ^a, J.A. Thompson ^c, A.A. Valishev ^a,
 Yu.V. Yudin ^a, A.S. Zaitsev ^{a,b}, S.G. Zverev ^a

^a*Budker Institute of Nuclear Physics, Novosibirsk, 630090, Russia*

^b*Novosibirsk State University, Novosibirsk, 630090, Russia*

^c*University of Pittsburgh, Pittsburgh, PA 15260, USA*

Abstract

The cross section of the process $e^+e^- \rightarrow \pi^0\pi^0\gamma$ has been measured in the c.m. energy range 600–970 MeV with the CMD-2 detector. The following branching ratios have been determined: $\mathcal{B}(\rho^0 \rightarrow \pi^0\pi^0\gamma) = (5.2_{-1.3}^{+1.5} \pm 0.6) \times 10^{-5}$ and $\mathcal{B}(\omega \rightarrow \pi^0\pi^0\gamma) = (6.4_{-2.0}^{+2.4} \pm 0.8) \times 10^{-5}$. Evidence for the $\rho^0 \rightarrow f_0(600)\gamma$ decay has been obtained: $\mathcal{B}(\rho^0 \rightarrow f_0(600)\gamma) = (6.0_{-2.7}^{+3.3} \pm 0.9) \times 10^{-5}$. From a search for the process $e^+e^- \rightarrow \eta\pi^0\gamma$ the following upper limit has been obtained: $\mathcal{B}(\omega \rightarrow \eta\pi^0\gamma) < 3.3 \times 10^{-5}$ at 90% CL.

1 Introduction

Radiative transitions of vector mesons into two pseudoscalar mesons have been attracting attention since long ago as a possible test of various low energy theoretical models and a source of information on controversial scalar states [1,2,3,4,5,6,7,8,9,10,11,12,13]. After the reliable observation of the $f_0(980)$ and $a_0(980)$ states in the $\phi(1020)$ meson decays by SND [14] and CMD-2 [15], recently confirmed by KLOE [16], the interest moved to the ρ and ω meson decays.

Information on the $\rho(\omega)$ decays to the $\pi\pi\gamma(\eta\pi^0\gamma)$ final states is rather scarce. Because of the large background from the initial state radiation in the process $e^+e^- \rightarrow \pi^+\pi^-$, a search for $\rho(\omega)$ decays into the $\pi^+\pi^-\gamma$ final state is difficult and among many such experiments [17] only one succeeded in the observation of the decay $\rho^0 \rightarrow \pi^+\pi^-\gamma$ [18]. A long search for the $\omega \rightarrow \pi^0\pi^0\gamma$ decay (see [17] and references therein) finally proved successful for the GAMS Collaboration, which observed it in π^-p collisions with the branching fraction of $(7.4 \pm 2.5) \times 10^{-5}$ [19]. Recently a high statistics study of the $\rho(\omega)$ energy range has been performed by the SND Collaboration [20,21]. They observe both ρ and ω decays into $\pi^0\pi^0\gamma$ with a branching ratio higher than that predicted by vector dominance. While for the ρ meson the excess can be explained by the $\rho^0 \rightarrow f_0(600)\gamma$ decay, first evidence for which is reported by SND, the reasons for the higher probability of the corresponding ω decay are not yet clear.

In our recent paper [22] we described a study of the process $e^+e^- \rightarrow \pi^0\pi^0\gamma$ in the c.m. energy range 920–1380 MeV, i.e. above the threshold of $\omega\pi^0$ production, using the CMD-2 detector at the VEPP-2M e^+e^- collider. In this work we report on the measurement of the cross section of the process $e^+e^- \rightarrow \pi^0\pi^0\gamma$ in the c.m. energy range 600–970 MeV with CMD-2. Also described is the first search for the process $e^+e^- \rightarrow \eta\pi^0\gamma$ in this energy range.

2 Experiment

The general purpose detector CMD-2 has been described in detail elsewhere [23]. Its tracking system consists of a cylindrical drift chamber (DC) and double-layer multiwire proportional Z-chamber, both also used for the trigger, and both inside a thin ($0.38 X_0$) superconducting solenoid with a field of 1 T. The barrel CsI calorimeter with a thickness of $8.1 X_0$ placed outside the solenoid has energy resolution for photons of about 9% in the energy range from 100 to 700 MeV. The angular resolution is of the order of 0.02 radians. The end-cap BGO calorimeter with a thickness of $13.4 X_0$ placed inside the solenoid has energy and angular resolution varying from 9% to 4% and from 0.03 to 0.02

radians, respectively, for the photon energy in the range 100 to 700 MeV. The barrel and end-cap calorimeter systems cover a solid angle of $0.92 \times 4\pi$ radians.

This analysis is based on a data sample corresponding to integrated luminosity of 7.7 pb^{-1} collected in 1998–2000 in the energy range 600–970 MeV. The step of the c.m. energy scan varied from 0.5 MeV near the ω peak to 5 MeV far from the resonance. The beam energy spread is about 4×10^{-4} of the total energy. The luminosity is measured using events of Bhabha scattering at large angles [24].

We use Monte Carlo simulation (MC) to model the response of the detector and determine the efficiency. Due to the beam background additional (“fake”) clusters can appear in the calorimeter. The corresponding probability as well as photon energy and angular spectra are obtained directly from the data using the process $e^+e^- \rightarrow \pi^+\pi^-\pi^0$. Then these photons are mixed with the detector response during simulation.

3 Data analysis

At the initial stage, we select events which have no tracks in the DC, five photons, the total energy deposition $1.7 < E_{\text{tot}}/E_{\text{beam}} < 2.2$, the total momentum $P_{\text{tot}}/E_{\text{beam}} < 0.3$ and at least three photons detected in the CsI calorimeter. The minimum photon energy is 30 MeV for the CsI and 40 MeV for the BGO calorimeter. Then a kinematic fit requiring energy-momentum conservation is performed with an additional reconstruction of two π^0 mesons. We require good reconstruction quality ($\chi^2 < 5$) and the ratio of the reconstructed to measured energy to be $0.75 < \omega_i/E_i < 1.8$ for each photon. After this stage 219 events remain in the whole energy range.

The dominant background comes from the processes

$$e^+e^- \rightarrow \eta\gamma, \quad \eta \rightarrow 3\pi^0, \tag{1}$$

$$e^+e^- \rightarrow \pi^0\gamma, \tag{2}$$

$$e^+e^- \rightarrow 3\gamma, \quad 4\gamma. \tag{3}$$

Events from the process (1) can imitate signal events if two soft photons are lost. The processes (2,3) can meet the selection criteria with one or two additional (“fake”) photons coming from shower splitting, “noisy” electronic channels in the calorimeter and beam background.

To determine the background contribution, the following procedure is used. All above listed processes are simulated using the Monte Carlo. To decrease

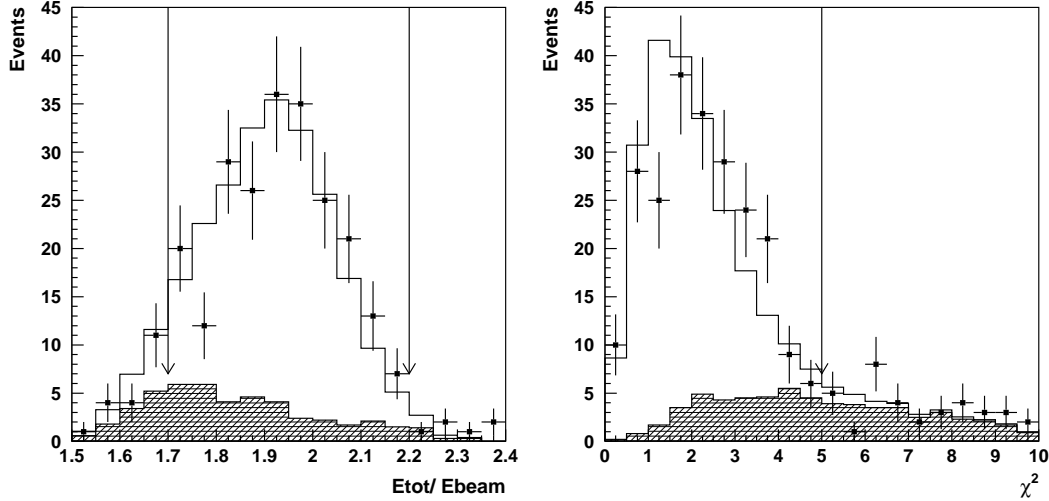


Fig. 1. The E_{tot} (left) and χ^2 distributions. The points with error bars represent experimental events, hatched histograms show the MC simulation for the background processes and open histograms are a sum of the signal and background MC. The arrows indicate the cuts imposed.

a statistical uncertainty, ten times more events than is expected from the background cross section and luminosity are used at each energy. Then the same selection criteria as for the data are applied. The obtained number of selected events is divided by ten and subtracted from experimental data at each energy. In total, about 29 background events are expected after this procedure.

Figure 1 shows the E_{tot} and χ^2 distribution for the data, signal and background MC. We use the χ^2 distributions to estimate the accuracy of the background estimation. The experimental distribution was fitted by a sum of MC and background. The ratio $N_{\text{bg}}^{\text{exp}}/N_{\text{bg}}^{\text{MC}} = 1.2 \pm 0.2$ was obtained. We conclude that the background level is estimated well and its systematic error does not exceed 40%. This results in a 6% systematic uncertainty in the cross section.

3.1 Approximation of the cross sections

At each energy point the cross section of the process σ is calculated from the observed number of events and background MC expectation using the following formula:

$$\sigma(\sqrt{s}) = \frac{N_{\text{exp}} - N_{\text{bg}}}{L\varepsilon(1 + \delta)}, \quad (4)$$

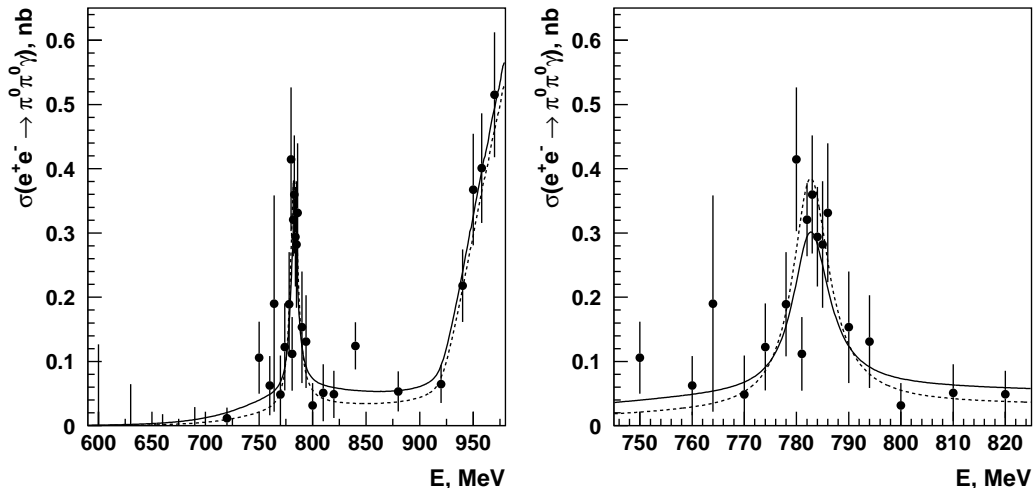


Fig. 2. The cross section of the process $e^+e^- \rightarrow \pi^0\pi^0\gamma$. The points with error bars represent the experimental data, while the solid and dashed curves correspond to the results of the fit I and III, respectively.

where N_{exp} is the number of observed events, N_{bg} is the expected number of background events from MC, L is the integrated luminosity, ε is the detection efficiency and $(1 + \delta)$ is the radiative correction at the corresponding energy.

To calculate the detection efficiency, we use Monte Carlo simulation taking into account the neutral trigger (NT) efficiency. NT is based on the information from the CsI calorimeter and its efficiency depends on the number of clusters and total energy deposition. The NT efficiency is estimated using events of the process $e^+e^- \rightarrow \pi^+\pi^-\pi^0$. We require the charged trigger signal and three or more clusters in the CsI calorimeter, and study the NT efficiency as a function of the energy deposition in CsI. The NT efficiency varies from 85% at c.m. energy 600 MeV to about 95% at 980 MeV.

The radiative corrections are calculated according to [27]. The dependence of the detection efficiency on the energy of the emitted photon is determined from simulation.

The obtained Born cross section of the process $e^+e^- \rightarrow \pi^0\pi^0\gamma$ is shown in Fig. 2 while Table 1 lists detailed information on the analysis of this reaction. No events were selected in the energy range 600 to 690 MeV, therefore our results are presented as upper limits at 90% C.L. The Feldman-Cousins procedure [25] was used to calculate errors (upper limits) at each energy. This cross section (the “dressed” one from the column VII) was used in the approximation of the energy dependence with resonances.

Meanwhile, for applications to various dispersion integrals like that for the leading order hadronic contribution to the muon anomalous magnetic mo-

Table 1

The c.m. energy, integrated luminosity, detection efficiency, number of observed events, background expectation, radiative correction, Born cross section σ , vacuum polarization correction and “bare” cross section $\hat{\sigma}$ of the process $e^+e^- \rightarrow \pi^0\pi^0\gamma$.

\sqrt{s} , MeV	L , nb $^{-1}$	ε , %	N_{exp}	N_{bg}	$1 + \delta$	σ , pb	$ 1 - \Pi(s) ^2$	$\hat{\sigma}$, pb
600	56.1	10.9	0	0.2	0.892	< 411	0.993	< 408
630	115.1	11.9	0	0.1	0.888	< 192	0.995	< 191
660	235.5	12.8	0	0.4	0.884	< 80	0.997	< 80
690	196.2	13.5	0	0.2	0.880	< 96	0.999	< 96
720	419.7	14.1	1	0.4	0.879	< 76	0.999	< 76
750	210.5	14.7	3	0.1	0.884	106^{+84}_{-68}	0.994	105^{+83}_{-68}
760	206.5	14.9	2	0.3	0.885	62^{+82}_{-38}	0.991	62^{+81}_{-38}
764	39.7	14.9	1	0.0	0.883	191^{+334}_{-120}	0.990	189^{+331}_{-119}
770	109.2	15.0	1	0.3	0.872	< 284	0.991	< 282
774	195.3	15.1	4	0.9	0.852	123^{+110}_{-66}	0.994	122^{+109}_{-66}
778	199.1	15.2	6	1.3	0.817	190^{+132}_{-88}	0.994	189^{+131}_{-87}
780	194.7	15.2	11	1.1	0.801	417^{+161}_{-92}	0.983	410^{+158}_{-90}
781	255.7	15.2	5	1.5	0.798	112^{+90}_{-41}	0.971	109^{+87}_{-40}
782	631.0	15.3	30	5.1	0.803	322^{+62}_{-59}	0.958	309^{+60}_{-57}
783	275.7	15.3	15	2.6	0.815	361^{+126}_{-107}	0.946	342^{+119}_{-101}
784	337.2	15.3	16	3.3	0.835	295^{+111}_{-85}	0.937	276^{+104}_{-80}
785	198.8	15.3	9	1.6	0.859	283^{+145}_{-102}	0.932	264^{+135}_{-95}
786	190.8	15.3	10	1.4	0.885	332^{+147}_{-124}	0.932	309^{+137}_{-116}
790	149.4	15.4	4	0.6	0.966	153^{+125}_{-75}	0.939	144^{+117}_{-70}
794	178.7	15.5	4	0.4	1.000	130^{+100}_{-60}	0.944	123^{+94}_{-57}
800	261.7	15.6	2	0.7	1.010	32^{+55}_{-24}	0.948	30^{+52}_{-23}
810	247.3	15.8	3	1.0	1.006	51^{+59}_{-40}	0.950	48^{+56}_{-38}
820	295.7	15.9	3	0.7	1.001	49^{+49}_{-34}	0.951	46^{+46}_{-32}
840	602.8	16.3	13	0.8	0.999	124^{+44}_{-38}	0.953	118^{+42}_{-36}
880	375.4	17.1	4	0.6	0.984	54^{+37}_{-26}	0.958	51^{+35}_{-25}
920	458.2	18.1	6	1.1	0.901	65^{+44}_{-29}	0.964	63^{+42}_{-28}
940	327.8	18.7	12	0.5	0.854	219^{+82}_{-60}	0.966	212^{+79}_{-58}
950	226.1	19.1	14	0.4	0.855	369^{+117}_{-100}	0.968	357^{+113}_{-97}
958	250.0	19.3	17	0.3	0.859	402^{+116}_{-101}	0.969	390^{+112}_{-98}
970	249.8	19.8	23	0.9	0.867	516^{+116}_{-101}	0.972	502^{+112}_{-98}

ment, the “bare” cross section should be used. Following the procedure in Ref. [26], the latter is obtained from the “dressed” one by multiplying it by the vacuum polarization correction $|1 - \Pi(s)|^2$, where $\Pi(s)$ is the photon polarization operator calculated taking into account the effects of both leptonic and hadronic vacuum polarization. The values of the correction and the “bare” cross section $\hat{\sigma}$ are presented in two last columns of Table 1.

The maximum likelihood method is applied to fit the experimental data obtained from the relation (4). We parameterize the amplitude of the process by a sum of the ρ and ω contributions. The former contains the $\rho \rightarrow \omega\pi^0$ transition plus one more mechanism beyond the vector dominance model which is chosen to be the $\rho^0 \rightarrow f_0(600)\gamma$ one. Because of the small width of the ω meson, the $\rho \rightarrow \omega\pi^0$ amplitude is rapidly falling below the $\omega\pi^0$ threshold, making thereby the $\rho^0 \rightarrow \omega\pi^0$ and $\rho^0 \rightarrow f_0(600)\gamma$ transitions distinguishable. On the contrary, the small width of the ω meson prevents from distinguishing various mechanisms possibly existing in the $\omega \rightarrow \pi^0\pi^0\gamma$ decay. For this reason we parameterize the ω meson amplitude by the $\omega \rightarrow \rho\pi$ transition only.

The Born cross section of the process is written as:

$$\sigma_{\pi^0\pi^0\gamma}(s) = \int |A_{\pi^0\pi^0\gamma}(s)|^2 d\Phi, \quad (5)$$

where $d\Phi$ is the final state phase space and

$$A_{\pi^0\pi^0\gamma} = A_{\rho \rightarrow \omega\pi^0} \left(\frac{m_\rho^2}{D_\rho} + \alpha \frac{m_{\rho'}^2}{D_{\rho'}} \right) + A_{\rho \rightarrow f_0(600)\gamma} \frac{m_\rho^2}{D_\rho} + A_{\omega \rightarrow \pi^0\pi^0\gamma} \frac{m_\omega^2}{D_\omega}. \quad (6)$$

Here the first term describes the amplitude of the $e^+e^- \rightarrow \rho, \rho' \rightarrow \omega\pi^0$ transition, while the second and third ones are the $e^+e^- \rightarrow \rho \rightarrow f_0(600)\gamma$ and $e^+e^- \rightarrow \omega \rightarrow \rho\pi^0$ amplitudes. m_V is the mass and D_V is the propagator of the vector meson V given by $D_V(s) = s - m_V^2 + i\sqrt{s}\Gamma_V(s)$, $\Gamma_V(s)$ is the corresponding energy dependent width. The real parameter $\alpha = g_{\rho'\omega\pi}/g_{\rho\omega\pi}$ is the ratio of the coupling constants for the ρ and ρ' mesons. The $A_{\rho \rightarrow \omega\pi^0}$ amplitude, proportional to the coupling constant $g_{\rho\omega\pi}$ of the $\rho \rightarrow \omega\pi$ transition, is written as in our previous analysis above 1 GeV [22].

The coupling constant $g_{\rho\omega\pi}$ and the following branching ratios are used as fit parameters:

$$\begin{aligned} \mathcal{B}(\rho^0 \rightarrow f_0(600)\gamma \rightarrow \pi^0\pi^0\gamma) &= \frac{1}{\sigma_\rho} \int |A_{\rho \rightarrow f_0(600)\gamma}(m_\rho)|^2 d\Phi, \\ \mathcal{B}(\omega \rightarrow \pi^0\pi^0\gamma) &= \frac{1}{\sigma_\omega} \int |A_{\omega \rightarrow \pi^0\pi^0\gamma}(m_\omega)|^2 d\Phi. \end{aligned} \quad (7)$$

Table 2
The fit results in various models

Fit parameters	Fit I	Fit II	Fit III
$\mathcal{B}(\omega \rightarrow \pi^0 \pi^0 \gamma), 10^{-5}$	$6.4_{-2.0}^{+2.4} \pm 0.8$	$6.2_{-2.0}^{+2.4} \pm 0.7$	$11.8_{-1.9}^{+2.1} \pm 1.4$
$g_{\rho\omega\pi}, \text{GeV}^{-1}$	$\equiv 16.7$	16.2 ± 1.4	18.6 ± 1.1
$\mathcal{B}(\rho \rightarrow f_0(600)\gamma \rightarrow \pi^0 \pi^0 \gamma), 10^{-5}$	$2.0_{-0.9}^{+1.1} \pm 0.3$	$2.3_{-1.2}^{+1.4} \pm 0.3$	$\equiv 0$
$\mathcal{B}(\rho \rightarrow \pi^0 \pi^0 \gamma), 10^{-5}$	$5.2_{-1.3}^{+1.5} \pm 0.6$	$5.4_{-1.4}^{+1.6} \pm 0.6$	$2.2 \pm 0.3 \pm 0.3$
$\chi^2 / \text{n. d. f.}$	19.2 / 28	19.0 / 27	26.7 / 28

Then the total branching fraction of the $\rho^0 \rightarrow \pi^0 \pi^0 \gamma$ decay is calculated from the following formula:

$$\mathcal{B}(\rho \rightarrow \pi^0 \pi^0 \gamma) = \frac{1}{\sigma_\rho} \int |A_{\rho \rightarrow \omega \pi^0}(m_\rho) + A_{\rho \rightarrow f_0(600)\gamma}(m_\rho)|^2 d\Phi. \quad (8)$$

In (7) and (8) σ_V is the cross section at the resonance peak without taking into account other contributions:

$$\sigma_V = \sigma_{e^+e^- \rightarrow V \rightarrow \pi^0 \pi^0 \gamma}(m_V^2) = \frac{12\pi \mathcal{B}(V \rightarrow e^+e^-) \mathcal{B}(V \rightarrow \pi^0 \pi^0 \gamma)}{m_V^2}, \quad (9)$$

$\mathcal{B}(V \rightarrow e^+e^-)$ and $\mathcal{B}(V \rightarrow \pi^0 \pi^0 \gamma)$ are the corresponding branching ratios.

3.2 Results of the fits

In all the following fits the ρ , ω and ρ' meson masses and widths are fixed at the world average values [17]. The $f_0(600)$ mass and width are badly known [17]. Therefore, we use a wide range of these parameters: $M_{f_0(600)} = 400\text{--}800$ MeV, $\Gamma_{f_0(600)} = 300\text{--}600$ MeV. For the ρ and ρ' resonances the energy dependence of the total width was described similarly to Ref. [22] while for the ω meson the total width was assumed to be energy independent. We perform three main fits: with $g_{\rho\omega\pi}$ equal to the value $(16.7 \pm 0.4 \pm 0.6) \text{GeV}^{-1}$ obtained in our analysis above 1 GeV [22] (fit I), with free $g_{\rho\omega\pi}$ (fit II) and without a contribution from the $\rho^0 \rightarrow f_0(600)\gamma$ decay (fit III). The results of the fits are shown in Table 2 and in Fig. 2 by the curves.

The value of the coupling constant $g_{\rho\omega\pi} = 16.2 \pm 1.4$ obtained in the second fit is in good agreement with the one from our measurement of the $e^+e^- \rightarrow \omega \pi^0$ cross section above 1 GeV [22].

The fits taking into account the $\rho^0 \rightarrow f_0(600)\gamma$ decay mode (fits I and II) better

describe data. The branching fraction $\mathcal{B}(\rho^0 \rightarrow f_0(600)\gamma)$ differs from zero by two standard deviations. However, the fit III also has good $\chi^2/\text{n. d. f.} = 26.7/28$. There are additional reasons to choose a fit with the $\rho \rightarrow f_0(600)\gamma$ decay:

- The branching fraction of the $\omega \rightarrow \pi^0\pi^0\gamma$ decay obtained in the fit III, $\mathcal{B}(\omega \rightarrow \pi^0\pi^0\gamma) = (11.8_{-1.9}^{+2.1} \pm 1.4) \times 10^{-5}$ is above the GAMS result $(7.4 \pm 2.5) \times 10^{-5}$ [19] by two standard deviations. The latter result obtained in π^-p collisions has no ρ contribution.
- The value of the coupling constant $g_{\rho\omega\pi} = 18.6 \pm 1.1$ obtained in the fit III is above that from our analysis above 1 GeV [22] by almost two standard deviations.
- The recent analysis of the process $e^+e^- \rightarrow \pi^0\pi^0\gamma$ by SND [21] also showed evidence for the $\rho^0 \rightarrow f_0(600)\gamma$ decay.

Thus, we choose the first model as our final result. The $\rho^0 \rightarrow f_0(600)\gamma$ branching fraction is calculated from the results listed in Table 2 taking into account that $\mathcal{B}(f_0(600) \rightarrow \pi^0\pi^0) = 1/3$.

3.3 Invariant mass spectrum

Figure 3 shows the spectrum of a $\pi^0\pi^0$ invariant mass for experimental events from the ω meson energy range (770–800 MeV). The experimental distribution agrees well with the $\omega \rightarrow \rho\pi^0$ decay model, however, the contribution from the $\omega \rightarrow f_0(600)\gamma$ decay is also acceptable. The existing statistics is not enough to distinguish these contributions, therefore we obtain only the total branching fraction of the $\omega \rightarrow \pi^0\pi^0\gamma$ decay.

3.4 Search for the decay $\omega \rightarrow \eta\pi^0\gamma$

For a search of events of the process $e^+e^- \rightarrow \eta\pi^0\gamma$ we first apply the same criteria as for the preliminary selection of $e^+e^- \rightarrow \pi^0\pi^0\gamma$ events. After that a kinematic fit requiring energy-momentum conservation is performed with the additional reconstruction of one soft π^0 meson and a good reconstruction quality, $\chi^2 < 6$, is required. To reject the dominant background from the process $e^+e^- \rightarrow \pi^0\pi^0\gamma$, we perform an additional kinematic fit with the $\pi^0\pi^0\gamma$ hypothesis and reject events that are consistent with it, $\chi_{\pi^0\pi^0\gamma}^2 < 6$. Then we look for a possible η signal in the invariant mass of two hard photons of the remaining three, $M_{\gamma\gamma}$. The $M_{\gamma\gamma}$ distribution is approximated with a Gaussian for the signal and a polynomial function for the background. The Gaussian mean value and width are fixed from the MC simulation of the signal events. The background shape is obtained using the $\pi^0\pi^0\gamma$ MC. In all energy

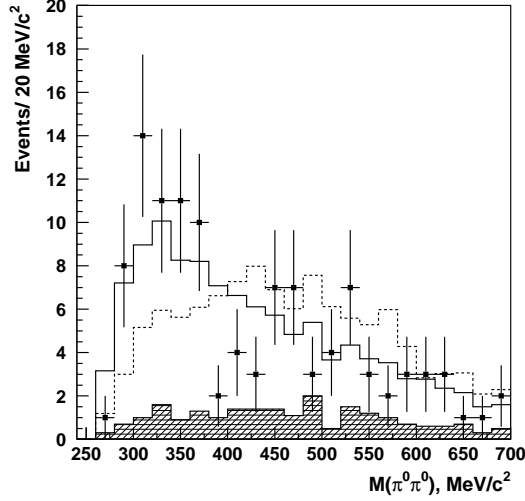


Fig. 3. The invariant mass of two π^0 mesons in the ω meson energy range. The points with error bars represent the experimental data, the solid histogram shows the MC simulation of the $\omega \rightarrow \rho\pi^0$ decay, the dashed one corresponds to the $\omega \rightarrow f_0(600)\gamma$ decay. The hatched histogram is the estimated background contribution.

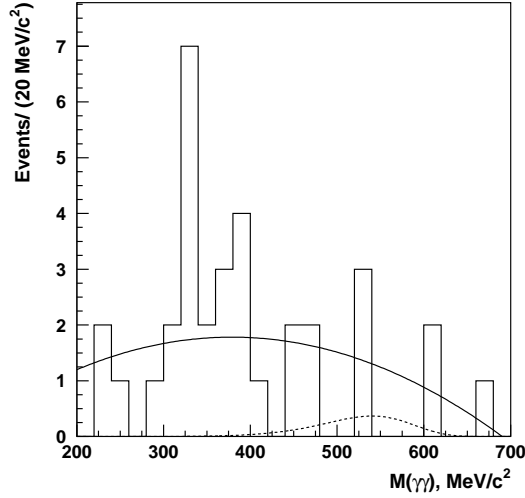


Fig. 4. The $M_{\gamma\gamma}$ distribution for the $\eta\pi^0\gamma$ candidates. The histogram represents experimental events and the solid curve shows the fit result. The dashed curve corresponds to the $\eta\pi^0\gamma$ MC.

ranges the resulting $\eta\pi^0\gamma$ signal is consistent with zero. Figure 4 shows the $M_{\gamma\gamma}$ distribution for events from the ω resonance region: $381 \text{ MeV} < E_{\text{beam}} < 401 \text{ MeV}$. The 90% CL upper limit for the number of $\eta\pi^0\gamma$ events is obtained: $N_{\eta\pi^0\gamma} < 2.4$. Using the detection efficiency of 1.3%, we set the following upper limit for the $e^+e^- \rightarrow \eta\pi^0\gamma$ cross section:

$$\sigma(e^+e^- \rightarrow \eta\pi^0\gamma) < 57 \text{ pb}, \quad (10)$$

Table 3
Main sources of systematic errors

Source	Contribution, %
Selection criteria	8
Background subtraction	6
Model uncertainty	5
Luminosity	2
Trigger efficiency	2
Radiative corrections	1
Total	12

and for the branching fraction of the ω meson:

$$\mathcal{B}(\omega \rightarrow \eta\pi^0\gamma) < 3.3 \times 10^{-5}. \quad (11)$$

3.5 Systematic errors

The main sources of systematic uncertainties in the cross section determination are listed in Table 3. The systematic error due to selection criteria is obtained by varying the photon energy threshold, total energy deposition, total momentum, and χ^2 . The model uncertainty corresponds to different detection efficiencies for the $\omega\pi^0$, $\rho\pi^0$ and $f_0(600)\gamma$ intermediate states. It also includes dependence on the $f_0(600)$ mass and width. The uncertainty in the determination of the integrated luminosity comes from the selection criteria of Bhabha events, radiative corrections and calibrations of DC and CsI. The error of the NT efficiency was estimated by trying various fitting functions for the energy dependence and variations of the cluster threshold. The uncertainty of the radiative corrections comes from the dependence on the emitted photon energy and the accuracy of the theoretical formulae. The resulting systematic uncertainty of the cross section in Table 1 as well as of the branching fractions in Table 2 is 12%.

4 Discussion

The obtained values of the branching fractions, $\mathcal{B}(\rho^0 \rightarrow \pi^0\pi^0\gamma) = (5.2_{-1.3}^{+1.5} \pm 0.6) \times 10^{-5}$ and $\mathcal{B}(\omega \rightarrow \pi^0\pi^0\gamma) = (6.4_{-2.0}^{+2.4} \pm 0.8) \times 10^{-5}$, are in good agreement with the previous measurements by GAMS [19] and SND [21]. Both values are significantly higher than those predicted by the vector dominance model

Table 4

Predictions for branching fractions of $\rho, \omega \rightarrow \pi^0\pi^0\gamma, \eta\pi^0\gamma$ decays.

Mode	Branching fraction
$\rho^0 \rightarrow \pi^0\pi^0\gamma$	$(1.1-4.7) \times 10^{-5}$
$\omega \rightarrow \pi^0\pi^0\gamma$	$(1.4-8.2) \times 10^{-5}$
$\rho^0 \rightarrow \eta\pi^0\gamma$	$2 \times 10^{-10} - 4 \times 10^{-6}$
$\omega \rightarrow \eta\pi^0\gamma$	$8.3 \times 10^{-8} - 6.3 \times 10^{-6}$

with the standard value of the coupling constant: $\sim 1 \times 10^{-5}$ and $\sim 3 \times 10^{-5}$ [4], respectively. An attempt to explain the obtained branching ratios results in a high value of $g_{\rho\omega\pi}$ contradicting the other observations like, e.g., the experimental values of the $\omega \rightarrow \pi^+\pi^-\pi^0$ and $\omega \rightarrow \pi^0\gamma$ widths.

Theoretical papers on the subject [1,2,3,4,5,6,7,8,9,10,11,12,13] offer a broad choice of effects influencing the discussed decays. In addition to the $\omega\rho\pi$ transition they include: $\rho - \omega$ mixing, pion and kaon loops, various scalar ($f_0(600), f_0(980), a_0(980)$) and tensor ($f_2(1270)$ and $a_2(1320)$) intermediate mesons decaying into $\pi\pi$ ($\eta\pi$).

Predictions of these models differ rather strongly from each other reflecting various approaches applied by their authors [10]. While most of the recent papers agree that the observed value of the branching fraction for the $\rho^0 \rightarrow \pi^0\pi^0\gamma$ decay can be ascribed to the intermediate $f_0(600)$ state, the situation with the corresponding ω decay remains controversial. The corresponding ranges of the predicted values of branching fractions are summarized in Table 4. Note that from the upper limits for the non- $\omega\pi$ $\pi^0\pi^0\gamma$ cross section obtained by us at higher energy in Ref. [22] a significant contribution from the $f_0(980)\gamma$ or $f_2(1270)\gamma$ mechanisms appears not very likely.

Much higher data samples of the ρ and ω decays expected in experiments at the upgraded collider VEPP-2000 in Novosibirsk [28] will help to significantly improve our understanding of their radiative decays.

From the obtained results on the cross section of the radiative processes $e^+e^- \rightarrow \pi^0\pi^0\gamma, \eta\pi^0\gamma$ one can estimate a possible contribution of the previously unstudied radiative processes to the leading order hadronic correction to the muon anomalous magnetic moment. To this end we first calculate the contribution of the process $e^+e^- \rightarrow \pi^0\pi^0\gamma$ using the “bare” cross section, $\hat{\sigma}$, from Table 1 in the energy range below 920 MeV. The result contains a piece coming from the $\omega \rightarrow \pi^0\pi^0\gamma$ decay already taken into account in Ref. [29] in the whole ω meson contribution, $a_\mu^\omega = (37.96 \pm 1.07) \cdot 10^{-10}$. This ω meson contribution is subtracted from the value above using the branching ratio $\mathcal{B}(\omega \rightarrow \pi^0\pi^0\gamma)$ with the result $(6.08 \pm 0.82) \cdot 10^{-12}$. A possible contribution

from the process $e^+e^- \rightarrow \pi^+\pi^-\gamma$ is twice that of $e^+e^- \rightarrow \pi^0\pi^0\gamma$, so that

$$a_\mu^{LO,\pi\pi\gamma}(600 \text{ MeV} - 920 \text{ MeV}) = (18.2 \pm 2.5) \cdot 10^{-12}.$$

Adding the contribution from the $\eta\pi\gamma$ final state, we finally obtain:

$$a_\mu^{LO,rad}(600 \text{ MeV} - 920 \text{ MeV}) < 0.24 \cdot 10^{-10} \text{ at } 90\% \text{ CL}.$$

Adding the upper limit from the energy range 920 MeV – 2000 MeV obtained previously [22], we obtain

$$a_\mu^{LO,rad}(600 \text{ MeV} - 2000 \text{ MeV}) < 0.7 \cdot 10^{-10} \text{ at } 90\% \text{ CL}$$

or about 10% of the current uncertainty of $a_\mu^{LO,rad}$ [29].

5 Conclusions

The following results are obtained in this work:

- Using a data sample corresponding to integrated luminosity of 7.7 pb^{-1} , the cross section of the process $e^+e^- \rightarrow \pi^0\pi^0\gamma$ has been measured in the c.m. energy range 600–970 MeV. The values of the cross section are consistent with those obtained by the SND detector [21] and have the similar accuracy. The following branching ratios have been determined: $\mathcal{B}(\rho \rightarrow \pi^0\pi^0\gamma) = (5.2_{-1.3}^{+1.5} \pm 0.6) \times 10^{-5}$ and $\mathcal{B}(\omega \rightarrow \pi^0\pi^0\gamma) = (6.4_{-2.0}^{+2.4} \pm 0.8) \times 10^{-5}$.
- We confirm evidence for the $\rho \rightarrow f_0(600)\gamma$ decay with the branching fraction $\mathcal{B}(\rho \rightarrow f_0(600)\gamma) = (6.0_{-2.7}^{+3.3} \pm 0.9) \times 10^{-5}$ reported by the SND Collaboration [21].
- A first search for the process $e^+e^- \rightarrow \eta\pi^0\gamma$ was performed allowing to set the 90% CL upper limits: $\sigma(e^+e^- \rightarrow \eta\pi^0\gamma) < 57 \text{ pb}$ in the c.m. energy range 685–920 MeV and $\mathcal{B}(\omega \rightarrow \eta\pi^0\gamma) < 3.3 \times 10^{-5}$.
- A possible contribution of the studied radiative processes to the muon anomalous magnetic moment was estimated to be negligible.

The authors are grateful to the staff of VEPP-2M for the excellent performance of the collider, and to all engineers and technicians who participated in the design, commissioning and operation of CMD-2. This work is supported in part by grants DOE DEFG0291ER40646, NSF PHY-9722600, NSF PHY-0100468, INTAS 96-0624, RFBR-98-02-1117851 and RFBR-03-02-16843.

References

- [1] P. Singer, Phys. Rev. 128 (1962) 2789;
Erratum - ibid, 161 (1967) 1694.
- [2] F.M. Renard, Nuovo Cimento, 62A (1969) 475.
- [3] S. Fajfer and R.J. Oakes, Phys. Rev. D 42 (1990) 2392.
- [4] A. Bramon, A. Grau and G. Pancheri, Phys. Lett. B 283 (1992) 416;
A. Bramon, A. Grau and G. Pancheri, Phys. Lett. B 289 (1992) 97.
- [5] J. Prades, Z. Phys. C 63 (1994) 491.
- [6] E. Marco, S. Hirenzaki, E. Oset and H. Toki, Phys. Lett. B 470 (1999) 20.
- [7] A. Bramon, R. Escribano, J.L. Lucio Martinez and M. Napsuciale, Phys. Lett. B 517 (2001) 345.
- [8] D. Guetta and P. Singer, Phys. Rev. D 63 (2001) 017502.
- [9] A. Gokalp, Y. Sarac and O. Yilmaz, Eur. Phys. J. C 22 (2001) 327.
- [10] J.E. Palomar, S. Hirenzaki and E. Oset, Nucl. Phys. A 707 (2002) 161.
- [11] A. Gokalp, S. Solmaz and O. Yilmaz, Phys. Rev. D 67 (2003) 073007.
- [12] A. Gokalp, A. Kucukarslan and O. Yilmaz, Phys. Rev. D 67 (2003) 073008.
- [13] Y. Oh and H. Kim, hep-ph/007286, July 2003.
- [14] M.N. Achasov et al., Phys. Lett. B 438 (1998) 441.
M.N. Achasov et al., JETP Lett. 68 (1998) 573.
M.N. Achasov et al., Phys. Lett. B 440 (1998) 442.
- [15] R.R. Akhmetshin et al., Phys. Lett. B 462 (1999) 380.
- [16] A. Aloisio et al., Phys. Lett. B 536 (2002) 209.
A. Aloisio et al., Phys. Lett. B 537 (2002) 21.
- [17] K. Hagiwara et al., Phys. Rev. D 66 (2002) 010001.
- [18] I.B. Vasserman et al., Sov. J. Nucl. Phys. 47 (1988) 1035;
S.I. Dolinsky et al., Phys. Rep. 202 (1991) 99.
- [19] D.M. Alde et al., Phys. Lett. B 340 (1994) 122.
- [20] M.N. Achasov et al., JETP Lett. 71 (2000) 355.
- [21] M.N. Achasov et al., Phys. Lett. B 537 (2002) 201.
- [22] R.R. Akhmetshin et al., Phys. Lett. B 562 (2003) 173.
- [23] G. A. Aksenov et al., Preprint Budker INP 85-118, Novosibirsk, 1985;
E. V. Anashkin et al., ICFA Instr. Bulletin 5 (1988) 18.

- [24] R. R. Akhmetshin et al., Preprint Budker INP 99-11, Novosibirsk, 1999.
- [25] G.J. Feldman and R.D. Cousins, Phys. Rev. D 57 (1998) 3873.
- [26] R.R. Akhmetshin et al., Phys. Lett. B 527 (2002) 161.
- [27] E. A. Kuraev and V.S. Fadin, Sov. J. Nucl. Phys., 41 (1985) 466.
- [28] Yu.M. Shatunov, Proc. of EPAC 2000, Vienna, Austria, 2000, p.439.
- [29] M. Davier, S. Eidelman, A. Höcker, Z. Zhang, Eur. Phys. J. C 27 (2003) 497;
M. Davier, S. Eidelman, A. Höcker, Z. Zhang, hep-ph/0308213.